Journal of Mining and Metallurgy, 43 B (2007) 39 - 56

THERMODYNAMIC MODELING OF THE Fe-Mg-Si SYSTEM

Y. Du[#], J.R. Zhao, C. Zhang, H.L. Chen and L.J. Zhang

State Key Laboratory of Powder Metallurgy,
Central South University, Changsha, Hunan, 410083, P.R. China

Abstract

A thermodynamic modeling for the Fe-Mg-Si system is conducted. All of the experimental phase diagram and thermodynamic data available from the literature are critically reviewed and assessed using thermodynamic models for the Gibbs energies of individual phases. The thermodynamic parameters for ternary liquid as well as binary phases $\alpha FeSi_2$ (high-temperature form of $FeSi_2$) and FeSi showing noticeable solubilities for Mg are evaluated in the optimization. Comparisons between the calculated and measured phase diagrams show that the measured isothermal sections at 1600°, 1454°, 727° and 710°C, the observed regions of primary phases are satisfactorily accounted for by the thermodynamic description. The limited thermodynamic data concerning the activity of Mg in liquid at 1350°C are found to be inconsistent with the well established phase relations. The liquidus projection and reaction scheme for the entire Fe-Mg-Si system are also presented.

Keywords: Fe-Mg-Si phase diagram, thermodynamic calculation, liquidus projection, reaction scheme

1. Introduction

Mg-base alloys have been playing an important part in the aerospace and automotive industry [1] due to a combination of low density and high strength. Additionally, Mg-base casting alloys are widely used for the manufacture of many engine, brake and supporting pieces as a substitution for classical Al-

[#] ***Corresponding author:*** yong-du@mail.csu.edu.cn

doi:10.2298/JMMB0701039D

based alloys [2]. In the Mg-based industry, iron and steel containers are usually employed because no intermetallic compound exists in the Fe-Mg binary system and the mutual solubilities between the two metals are very low: negligible for Mg in solid iron and 0.018 at.% for Fe in liquid Mg at 727°C [3, 4]. Si, which forms dense and stable intermetallic compounds with both Fe and Mg and increases the difficulty to obtain high purity Mg-base alloys [5], is often found as an impurity accompanying iron and steel product [6]. Knowledge of phase diagram and thermodynamic properties in the Fe-Mg-Si system is a prerequisite for the development of multi-component Mg-base alloys [7].

There are several pieces of phase diagram and thermodynamic data on the Fe-Mg-Si system available in the literature. To the authors' knowledge, there is no publication on thermodynamic calculation for this ternary system due to the existence of a very complicated ternary liquid miscibility gap. The purposes of the present work are (i) to critically evaluate the measured phase diagram and thermodynamic data available for the Fe-Mg-Si system, and (ii) to obtain an optimal set of thermodynamic parameters for this ternary system over the whole composition and temperature ranges with a satisfactory description for the observed miscibility gap.

2. Evaluation of experimental phase diagram data

The experimental phase diagram and thermodynamic data for the Fe-Mg-Si system available in the literature were reviewed by Lebrun et al. [8]. The present assessment takes into account both the data assessed by Lebrun et al. [8] and those published later or not reviewed by them [8]. To facilitate reading, the symbols to denote the phases in the Fe-Mg-Si system are listed in Table 1. Because the αFe phase and δFe phase both have two structures (disordered Bcc_A2 phase and ordered Bcc_B2 phase), they are denoted as Bcc_A2 and Bcc_B2 in the phase diagram. In the reaction scheme, they are denoted as αFe. Using a combination of thermal analysis, metallography and X-ray diffraction patterns with Debye-Scherrer films, Zwicker [9] presented a liquidus surface in the Si-rich region. According to Zwicker [9], the liquidus surface is dominated with primary region of FeSi phase. Two invariant reactions were also reported [9]: $L + FeSi \Leftrightarrow Mg_2Si + \alpha FeSi_2$ at 1000°C and $L \Leftrightarrow (Si) + \alpha FeSi_2 + Mg_2Si$ at a temperature below 946°C. The existence of

a quasi-binary peritectic reaction, L + FeSi ⇔ Mg_2Si, was confirmed, and the temperature of this peritectic reaction was suggested to be above 1085°C by Zwicker [9]. The experimental information from Zwicker [9] is employed in the present optimization.

Table1. Symbols used to denote the phases in the Fe-Mg-Si system

Symbol	Phase
(Mg)	Solid solution based on Mg with Hcp_A3 structure
(Si)	Solid solution based on Si with Diamond_A4 structure
Bcc_A2	Solid solution based on Fe with disordered Bcc_A2 structure
Bcc_B2	Solid solution based on Fe with ordered Bcc_B2 structure
γFe	Solid solution based on Fe with Fcc_A1 structure
α$FeSi_2$	Solid solution based on high-temperature form of $FeSi_2$
β $FeSi_2$	Solid solution based on low-temperature form of $FeSi_2$
FeSi	Solid solution based on FeSi
Fe_2Si	Solid solution based on Fe_2Si
Mg_2Si	Solid solution based on Mg_2Si
L1	Liquid phase at high temperature or in Fe-rich region at low temperature
L2	Liquid phase in Mg-rich region at low temperature

By means of a vapor pressure measurement, Guichelaar et al. [10] investigated the miscibility gap between liquids in both Fe-rich and Mg-rich regions at 1454.5°C. Both the solubility of Mg in the Fe-rich liquid and that of Fe in the Mg-rich liquid at low silicon levels (5 to 17 mass% Si) were measured by Guichelaar et al. [10]. The reported tie-lines of the liquidus miscibility gap are utilized in this optimization.

Using a micro-oven with a Mo heater in an atmosphere of purified argon, the solubilities of Mg in the Fe-rich liquid at 1600°C were measured by Ageev and Archugov [11]. It is found that Si shows negligible effect on the solubility of Mg in the Fe-rich liquid within the investigated composition range. The liquidus curves in the Mg-rich corner were determined by both Rodyakin et al. [12] and Normann et al. [5]. Rodyakin et al. [12] determined the solubility of Fe in Mg at 800°C by measuring the solubility rate constant and the diffusion coefficient of Fe in Mg. Using the atomic absorption spectroscopy and electron microprobe analysis, Normann et al. [5] measured the solubilities of Fe in Mg-rich liquid at 670°, 710° and 750°C. The values published by Normann et al. [5] are in agreement with the calculated ones of the currently employed binary Fe-Mg system [3, 4], while those by Rodyakin et al. [12] are not. Consequently, the experimental data from Ageev and Archugov [11] and Normann et al. [5] are used in the present optimization.

Recently, Pierre et al. [6] carried out an extensive investigation on the solid-liquid phase equilibria in the Fe-Mg-Si system at 727°C by means of both Fe-Mg-Si powder mixtures and diffusion couples. Two three-phase regions, L + FeSi + Mg_2Si and L + FeSi + Bcc_B2, were observed. The experimental data from Pierre et al. [6] are utilized in the optimization.

In the literature, there is only one piece of thermodynamic data on the Fe-Mg-Si system. By means of the electromotive force (emf) method, Lepinskikh et al. [13] determined the activities of Fe, Mg and Si at 1350°C in liquid Fe-Mg-Si alloys. Preliminary thermodynamic modeling performed in the present work indicates that most of the activities given by Lepinskikh et al. [13] are inconsistent with the mentioned phase diagram data. As a consequence, only the activities of Mg along the vertical section of $x_{Fe}/x_{Si}=0.17$ are employed in the present optimization, where x_{Fe} and x_{Si} denote the mole fractions of Fe and Si, respectively.

3. Thermodynamic model

There are 11 stable phases in the Fe-Mg-Si system: Liquid, αFe, δFe, γFe, $\alpha FeSi_2$, $\beta FeSi_2$, Fe_2Si, FeSi, Mg_2Si, (Mg) and (Si). In the present modeling, the Gibbs energy functions for Fe, Mg and Si are taken from the SGTE compilation by Dinsdale [14]. The thermodynamic parameters of the Fe-Si,

Mg-Si, and Fe-Mg binary systems are taken from Lacaze and Sundman [15], Kevorkov et al. [16] and Ansara et al. [17], respectively. The calculated binary phase diagrams are presented in Figs. 1 to 3. In the following, the analytical expressions for the ternary phases are briefly presented.

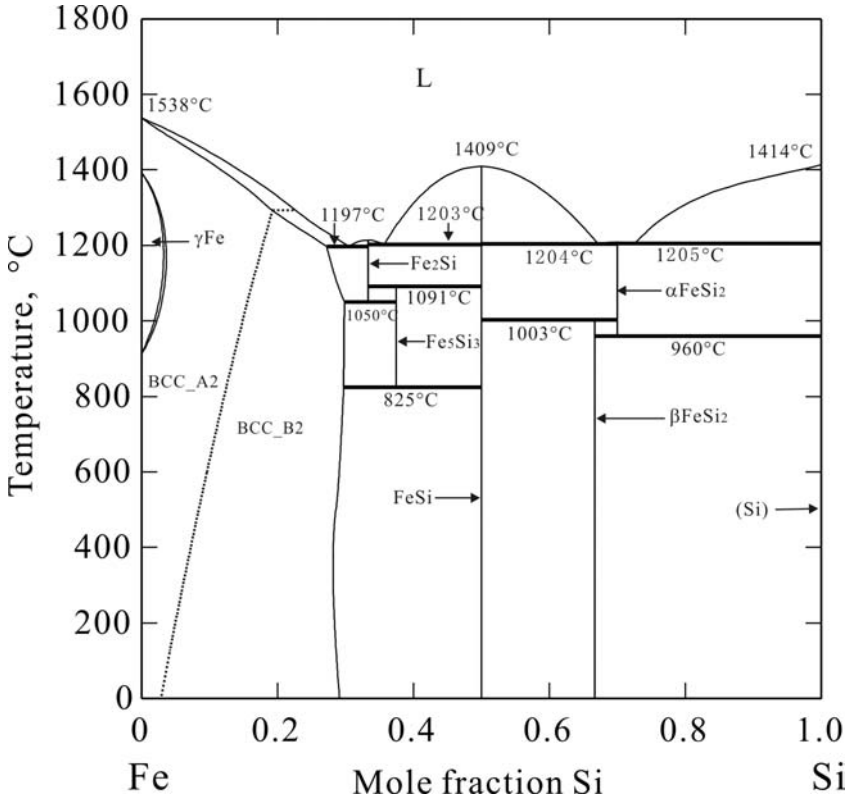

Fig. 1. Calculated Fe-Si phase diagram [15]

3.1 Liquid phase

The Gibbs energy of the ternary liquid phase is described by the Redlich-Kister polynomial [18]

$$
\begin{aligned}
{}^{0}G_m^L = {} & x_{Fe}\cdot {}^{0}G_{Fe}^L + x_{Mg}\cdot {}^{0}G_{Mg}^L + x_{Si}\cdot {}^{0}G_{Si}^L + R\cdot T(x_{Fe}\cdot \ln x_{Fe} + x_{Mg}\cdot \ln x_{Mg} + x_{Si}\cdot \ln x_{Si}) \\
& + x_{Fe}\cdot x_{Mg}\cdot L_{Fe,Mg}^L + x_{Fe}\cdot x_{Si}\cdot L_{Fe,Si}^L + x_{Mg}\cdot x_{Si}\cdot L_{Mg,Si}^L + {}^{ex}G_{Fe,Mg,Si}^L \qquad (1)
\end{aligned}
$$

in which R is the gas constant, and x_{Fe}, x_{Mg}, and x_{Si} are the mole fractions of Fe, Mg, and Si, respectively. The standard element reference (SER) state [14], i.e. the stable structure of the element at 25°C and 1 bar, is used as the reference state of the Gibbs energy. The parameters denoted as $L^{L}_{i,j}$ are the interaction parameters from the binary systems. The ternary excess Gibbs energy is expressed as follows:

$$ {}^{ex}G^{L}_{Fe,Mg,Si} = x_{Fe} \cdot x_{Mg} \cdot x_{Si} \cdot (x_{Fe} \cdot {}^{0}L^{L}_{Fe,Mg,Si} + x_{Mg} \cdot {}^{1}L^{L}_{Fe,Mg,Si} + x_{Si} \cdot {}^{2}L^{L}_{Fe,Mg,Si}) \qquad 2 $$

where the parameters ${}^{0}L^{L}_{Fe,Mg,Si}$, ${}^{1}L^{L}_{Fe,Mg,Si}$ and ${}^{2}L^{L}_{Fe,Mg,Si}$ are ternary interaction parameters to be optimized in the present work.

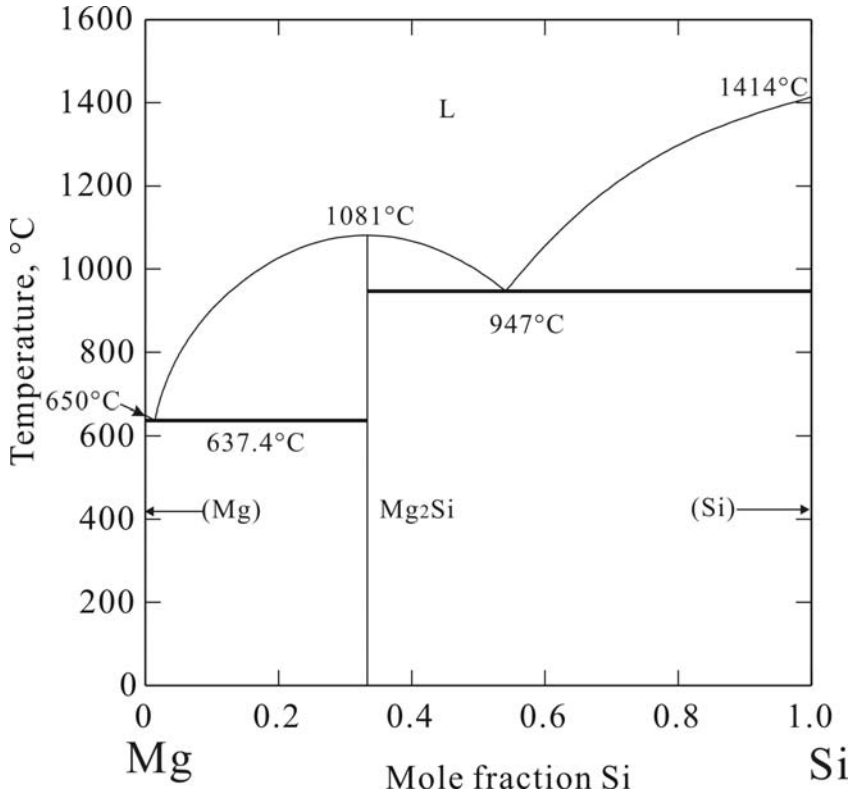

Fig. 2. Calculated Mg-Si phase diagram [16]

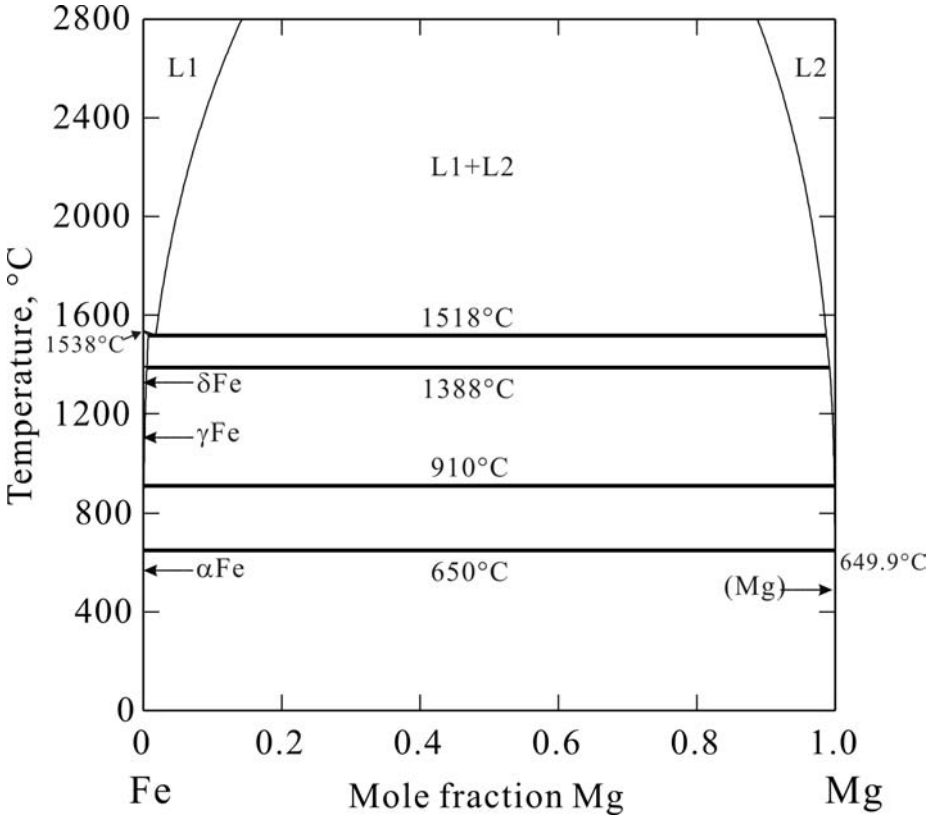

Fig. 3. Calculated Fe-Mg phase diagram [17]

3.2 Binary phases extending into the ternary system

Since the solubilities for Mg in $\alpha FeSi_2$ and FeSi were experimentally detected [9, 11], the sublattice models Fe_3 (Mg, **Si**)$_7$ and (Fe)$_1$ (Mg, **Si**)$_1$ are utilized to describe them, respectively. The boldfaces mean normal atoms (i.e. major species) in the sublattices. The Gibbs energy of $\alpha FeSi_2$ per mole formula is expressed as

$$
\begin{aligned}
{}^{0}G^{\alpha FeSi_2} - H^{SER} = {} & y_{Mg} \cdot {}^{0}G^{\alpha FeSi_2}_{Fe:Mg} + y_{Si} \cdot {}^{0}G^{\alpha FeSi_2}_{Fe:Si} + 7R \cdot T(y_{Mg} \cdot \ln y_{Mg} + y_{Si} \cdot \ln y_{Si}) \\
& + y_{Mg} \cdot y_{Si} \cdot L^{\alpha FeSi_2}_{Fe:Mg,Si}
\end{aligned} \tag{3}
$$

in which y_{Mg} and y_{Si} are the site fractions of Mg and Si on the second sublattice. The parameters denoted as ${}^{O}G_{i:j}^{\alpha FeSi_2}$ (also called compound energies) are the Gibbs energy of the end members.

The parameter $L_{Fe:Mg,Si}^{\alpha FeSi_2}$ represents the interactions of Mg and Si within the second sublattice. An analogous equation can be written for the Gibbs energy of FeSi phase. Due to the limited experimental information, $\beta FeSi_2$, Fe_2Si and Mg_2Si are treated as pure binary phases.

3.3 Model used for ordered/disordered phases

The ordered/disordered transition between Bcc_A2 and Bcc_B2 is described with the model $(Fe, Mg, Si, Va)_{0.5}(Fe, Mg, Si, Va)_{0.5}$, where Va means vacancy. In order to represent the Gibbs energies of the ordered/disordered phases using a single function, Bcc_A2 phase is described by the model $(Fe, Mg, Si, Va)_1$. Ansara et al. [19, 20] have derived an equation, which allows the thermodynamic properties of the disordered phase to be evaluated independently. This is done by resolving the Gibbs energy into the following three terms:

$$
\begin{aligned}
{}^{0}G_m^{\alpha\delta Fe} = {}& {}^{0}G_m^{A2}(x_{Fe}, x_{Mg}, x_{Si}) + {}^{0}G_m^{B2}(y'_{Fe}, y'_{Mg}, y'_{Si}, y''_{Fe}, y''_{Mg}, y''_{Si}) \\
& - {}^{0}G_m^{B2}(x_{Fe}, x_{Mg}, x_{Si}) \qquad (4)
\end{aligned}
$$

in which the notation $\alpha\delta Fe$ represents both Bcc_A2 and Bcc_B2 phases. y'_{Fe}, y'_{Mg} and y'_{Si} are the site fractions of Fe, Mg and Si in the first sublattice, and , y''_{Fe}, y''_{Mg} and y''_{Si} in the second one. ${}^{O}G_m^{A2}(x_{Fe}, x_{Mg}, x_{Si})$ is the Gibbs energy of the disordered Bcc_A2 phase. The second term ${}^{O}G_m^{B2}(y'_{Fe}, y'_{Mg}, y'_{Si}, y''_{Fe}, y''_{Mg}, y''_{Si})$ is described by the sublattice model and implicitly contains a contribution from the disordered state. The last term ${}^{O}G_m^{B2}(x_{Fe}, x_{Mg}, x_{Si})$ represents that contribution from the disordered state to the ordered one. When the site fractions are equal, i.e. $y'_{Fe} = y''_{Fe}$, $y'_{Mg} = y''_{Mg}$ and $y'_{Si} = y''_{Si}$, the last two terms cancel each other. In the present work, no ternary interaction

parameters are used for both Bcc_A2 and Bcc_B2 since no experimental data about both Bcc_A2 and Bcc_B2 were available in the literature.

4. Results and discussions

The evaluation of the model parameters is attained by recurrent runs of the PARROT program [21], which works by minimizing the square sum of the differences between experimental values and computed ones. In the assessment procedure, each piece of experimental information is given a certain weight. The weights were varied systematically during the assessment until most of the experimental data were accounted for within the estimated uncertainty limits.

For liquid, it is possible to optimize three interaction parameters, as shown in Eq. (2), because the liquid miscibility gap at 1454°C has been well established over the entire composition range. In order to account for the invariant equilibrium L + FeSi ⇔ $\alpha FeSi_2$ + Mg_2Si at 1000°C, one constant regular parameter ${}^{0}L^{\alpha FeSi_2}_{Fe:Mg,Si}$ was adjusted for $\alpha FeSi_2$. To reproduce the measured compositions for FeSi [11] associated with the three-phase equilibria, L + FeSi + Mg_2Si and L + FeSi + Bcc_B2, one regular parameter for FeSi is adjusted in the present optimization. The step-by-step optimization procedure described by Du et al. [22] in detail was utilized in the present assessment. The assessed thermodynamic parameters for the Fe-Mg-Si system are listed in Table 2.

Figures 4 to 7 show the calculated isothermal sections at 1600°, 1454°, 727° and 710°C along with the experimental data [5, 6, 10, 11]. To visualize the experimental data [5, 6] in Mg-rich region, two enlarged isothermal sections at 727°C and 710°C are shown in Figs. 6(b) and Fig. 7(b), respectively. As can be seen from those figures, all the reliable experimental

values are well reproduced by the present modeling. Additionally, two measured three-phase regions, L + FeSi + Mg_2Si and L +FeSi + Bcc_B2, can be seen in Figs. 6(a) and 7(a). The calculations are consistent with the experimental observations of Pierre et al. [6]. In Figs. 6(a) and 7(a), the boundaries between disordered Bcc_A2 and ordered Bcc_B2 phases are shown in the form of dotted lines.

*Table 2. Optimized thermodynamic parameters in the Fe-Mg-Si System**

Liquid: Model $(Fe, Mg, Si)_1$

$$^{ex}G^{L}_{Fe,Mg,Si} = x_{Fe}\cdot x_{Mg}\cdot x_{Si}(-62000\cdot x_{Fe} - 102000\cdot x_{Mg} - 65000\cdot x_{Si})$$

$\alpha FeSi_2$: Model $(Fe)_3(Mg, \mathbf{Si})_7$

$$^{0}G^{\alpha FeSi_2}_{Fe:Si} - 3\,^{0}G^{Bcc\_A2}_{Fe} - 7\,^{0}G^{Diamond\_A4}_{Si} = -196490 - 9.2\cdot T$$

$$^{0}G^{\alpha FeSi_2}_{Fe:Mg} - 3\,^{0}G^{Bcc\_A2}_{Fe} - 7\,^{0}G^{Hcp\_A3}_{Mg} = +3540$$

$$^{0}L^{\alpha FeSi_2}_{Fe:Mg,Si} = -240000$$

FeSi: Model $(Fe)_1(Mg, \mathbf{Si})_1$

$$^{0}G^{FeSi}_{Fe:Si} - {}^{0}G^{Bcc\_A2}_{Fe} - {}^{0}G^{Diamond\_A4}_{Si} = -72761.2+4.44\cdot T$$

$$^{0}G^{FeSi}_{Fe:Mg} - {}^{0}G^{Bcc\_A2}_{Fe} - {}^{0}G^{Hcp\_A3}_{Mg} = +3000$$

**In J/(mol of atom); temperature (T) in Kelvin. The Gibbs energies for the pure elements are from the SGTE compilation [14]. The thermodynamic parameters in the Fe-Si, Mg-Si, and Fe-Mg systems are taken from [15-17], respectively.*

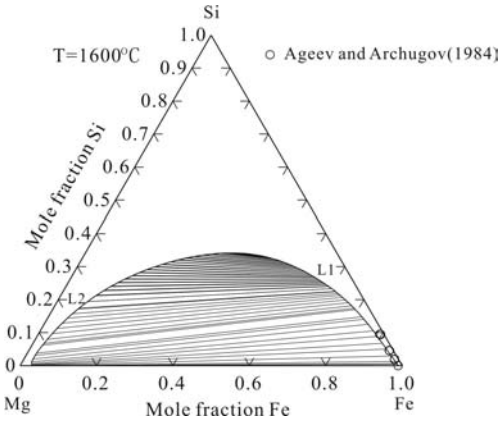

Fig. 4. Calculated isothermal section at 1600°C in the Fe-Mg-Si system,compared with the experimental data [11]

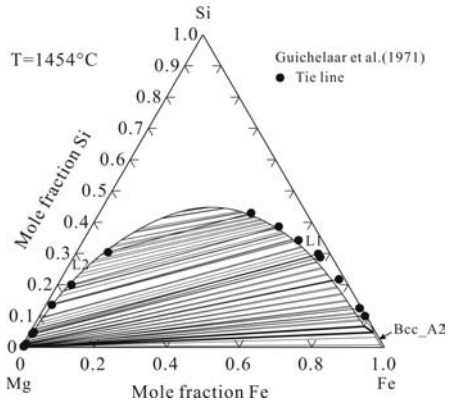

Fig. 5. Calculated isothermal section at 1454°C in the Fe-Mg-Si system along with the experimental data [10]

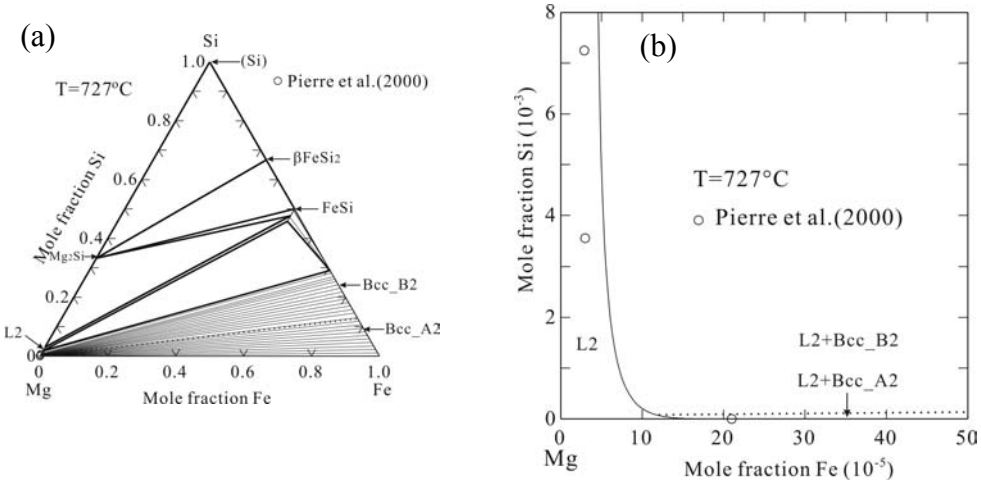

Fig. 6. (a) Calculated isothermal section at 727°C of the Fe-Mg-Si system compared with the experimental data [6]. (b) Enlarged Mg-rich region along with the experimental data [6]. The dotted line represents the boundary between Bcc_A2 and Bcc_B2

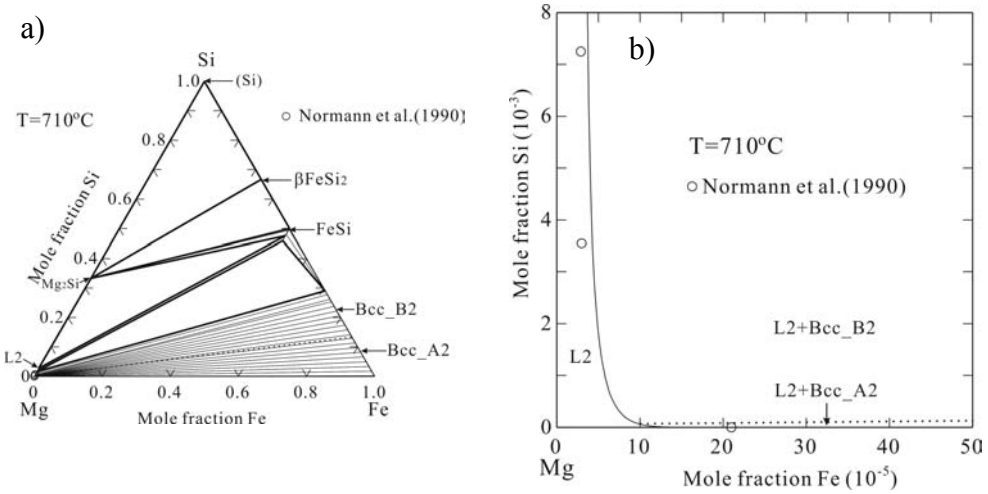

Fig. 7. (a) Calculated isothermal section at 710°C of the Fe-Mg-Si system compared with the experimental data [5]. (b) Enlarged Mg-rich region along with the experimental data [5]. The dotted line represents the boundary between Bcc_A2 and Bcc_B2

The calculated activities of Mg at 1350°C along the vertical section at x_{Fe}/x_{Si} =0.17 are shown in Fig. 8 together with the experimental data [13]. The calculation can satisfactorily account for the scattering experimental values within estimated experimental uncertainties, except for some deviations at high content of Mg. The major reason for this discrepancy is that the activities measured by Lepinskikh et al. [13] are inconsistent with the phase diagram data utilized in the present optimization. Consequently, the calculated activities of Mg along other vertical sections are not compared with the corresponding experimental data [13].

Figure 9(a) shows the calculated liquidus projection of the Fe-Mg-Si system. The existence of a large miscibility gap in the ternary system resulting from the miscibility gap in the binary Fe-Mg system is a distinctive feature of this ternary system. It should be noted that there is a demixing of the melts, L $\Leftrightarrow$ L1+L2. L1 denotes the Fe-rich liquid phase below the critical point associated with L $\Leftrightarrow$ L1+L2 as well as the liquid phase above that point, while L2 represents the Mg-rich liquid phase below the critical point. Two

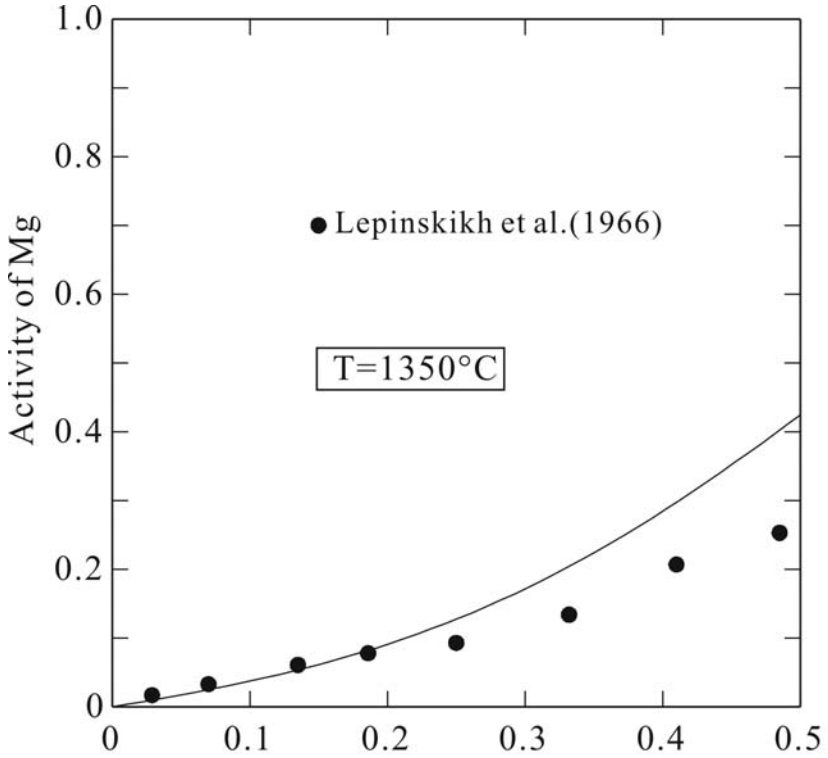

Fig. 8. Calculated activities of Mg along the vertical section of x_{Fe}/x_{Si}=0.17 compared with the experimental data [13]. The reference state is liquid Mg

four-phase monotectic reactions M_1 and M_2 in Fe-rich region were observed. M_1 and M_2 represent L1 ⇔ Fe_2Si + L2 + FeSi and L1 ⇔ Bcc_B2 + Fe_2Si + L2, respectively. M_2 appears twice on the liquid surface, once close to the Fe-Si binary side and once close to Mg-rich corner. The monotectic reactions M_2 and M_2' originate from the large miscibility gap in the binary Fe-Mg system, in which an invariant reaction, L1 ⇔ L2 + δFe, occurs with the liquid compositions at both L1 and L2. The monotectic reactions M_1 and M_1' result from the demixing of the liquid phase. As can be seen from Fig. 9(a), there is one common maximum point, which denoted as L1 ⇔ L2 + Fe_2Si, between M_1 and M_2, as well as between M_1' and M_2'. Figures 9(a) to (c) show the details

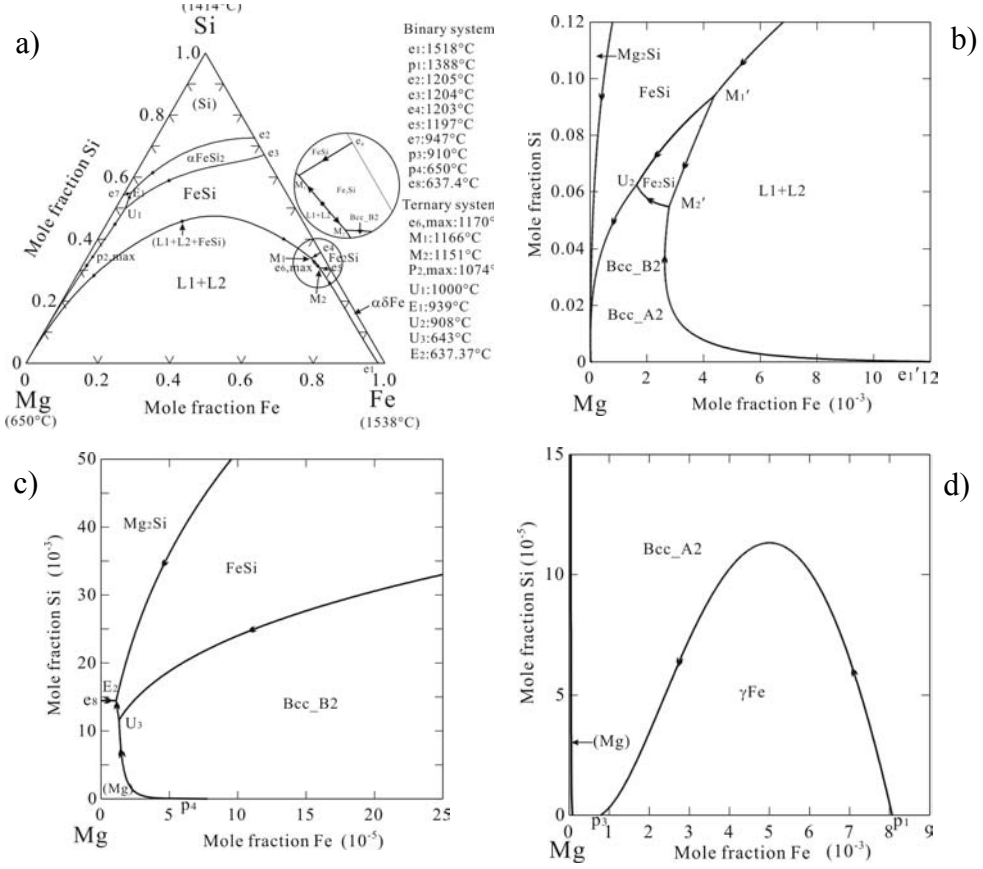

Fig. 9. Calculated liquidus projection of the Fe-Mg-Si system according to the present work. (a) in the whole composition range, (b) from 0 to 1.2 at.% Fe,(c) from 0 to 0.025 at.% Fe, (d) from 0 to 0.9 at.% Fe

of five invariant reactions in Mg-rich region. Using thermodynamic calculations, these details can be clearly revealed. The calculated invariant equilibria along with the experimental values [9] are listed in Table 3.

Finally, the reaction scheme for the entire Fe-Mg-Si system is shown in Fig. 10, which has been proved to be a useful tool in describing ternary and higher component systems. According to the present calculation, liquid phase decomposes into L1 + L2 + FeSi at the critical point of 1334°C. This behavior directly leads to the large miscibility gap in the Fe-Mg-Si system. Similar aspects in Al-Mg-Sc and Al-Bi-Zn systems have been observed [23, 24].

Table3. Calculated invariant reactions in the Fe-Mg-Si system, compared with the experimental data from literature

Source	Invariant equilibrium	Temperature (ºC)
	$L1 \Leftrightarrow Fe_2Si + FeSi + L2$	
Calculated (This work)		1166
	$L1 \Leftrightarrow \alpha\delta Fe + Fe_2Si + L2$	
Calculated (This work)		1151
	$L + FeSi \Leftrightarrow Mg_2Si + \alpha FeSi_2$	
Calculated (This work)		1000
Measured [9]		1000
	$L \Leftrightarrow \alpha FeSi_2 + (Si) + Mg_2Si$	
Calculated (This work)		939
Measured [9]		<946
	$L + Fe_2Si \Leftrightarrow FeSi + \alpha\delta Fe$	
Calculated (This work)		908
	$L + \alpha\delta Fe \Leftrightarrow (Mg) + FeSi$	
Calculated (This work)		643
	$L \Leftrightarrow FeSi + Mg_2Si + (Mg)$	
Calculated (This work)		637

5. Summary

Phase equilibrium data in the whole Fe-Mg-Si system available in the literature are critically reviewed. On the basis of reliable literature data, a self-consistent set of thermodynamic parameters for the Fe-Mg-Si system is obtained. Comprehensive comparisons show that most of the experimental data are well accounted for by the present description.

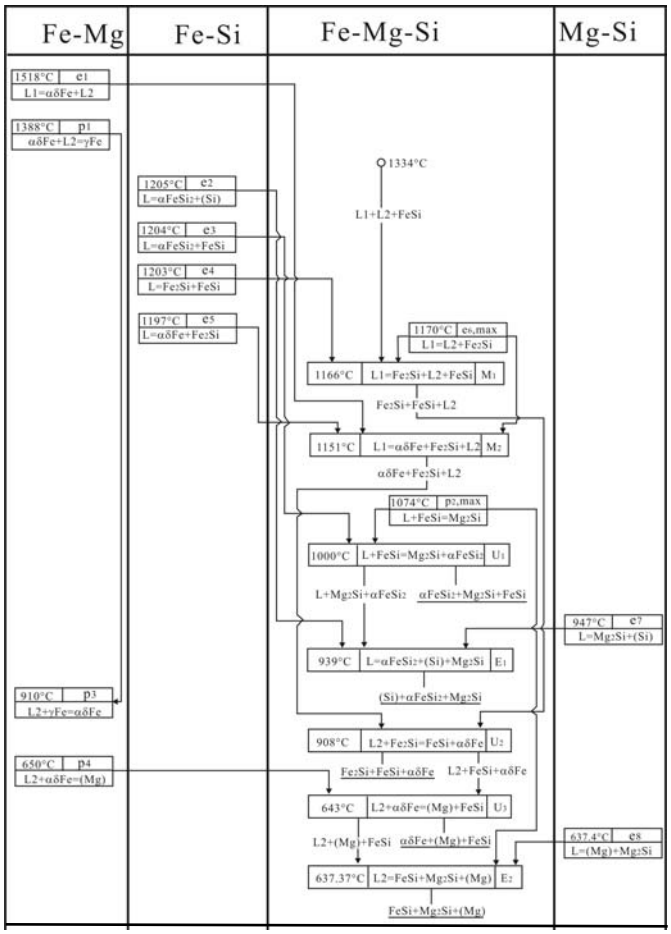

Fig. 10. Reaction scheme for the entire Fe-Mg-Si system according to the present work. L1 denotes the Fe-rich liquid phase below the critical point associated with L ⇔ L1+L2 as well as the liquid phase above that point, while L2 represents the Mg-rich liquid phase below the critical point

The liquidus projection and the reaction scheme of the Fe-Mg-Si system over the whole temperature and composition range have been constructed, which are of interest for engineering applications as well as basic materials research. The complicated invariant reactions associated with the miscibility gap in the Mg-rich and Fe-rich corners have been carefully described.

Acknowledgements

The financial support from the National Outstanding Youth Science Foundation of China (Grant No. 50425103), the National Natural Science Foundation of China (Grant No. 50571114) and the Hunan Provincial Natural Science Foundation of China (Grant No. 60JJ20010) is acknowledged. One of the authors (Yong Du) acknowledges the Cheung Kong Chair Professorship released by Ministry of Education of China. The donation of the Leica DMLP microscope from the Alexander von Humboldt Foundation is greatly appreciated.

References

1. S.Schumann, H.Friedirch, Mater.Sci.Forum, 51(2003)419.
2. K.U.Kainer, Magnesium Alloys and Technologies, Wiley-VCH, Weinheim, 2003.
3. T.B.Massalski, Binary Alloy Phase Diagrams, ASM International, Materials Park, OH, 1986.
4. T.Haitani, Y.Tamura, T.Motegi, N.Kono, H.Tamehiro, Mater.Sci.Forum, 697(2003)419.
5. H.H.Normann, H.Thoresen, J.E.Tibballs, C.J.Simensen, Proc. Conf. on Light Metals, Amsterdam, Netherlands, 1990, p.823.
6. D.Pierre, M.Peronnet, F.Bosselet, J.C.Viala, J.Bouix, J. Phase Equilib. Diffus., 21(2000)78.
7. J.Grobner, L.L.Rokhlin, T.V.Dobatkina, R.Schimid-Fetzer, J.Alloys Compd., (2006), 433(2007)108.
8. N.Lebrun, C.Baetzner, A.Stamou, J.Robinson, In: Ternary alloys. VCH, Weinheim, 2004. p.564.
9. V.Zwicker, Z.Metallkd., 45(1954)31.
10. P.J.Guichelaar, P.K.Trojan, R.A.Flinn, Metall.Trans., 2(1971)3305.
11. Y.A.Ageev, S.A.Archugov, Russ. Metall., 3(1984)78.
12. V.V.Rodyakin, A.E.Andreyev, V.S.Tkalich, Russ.Metall., 3(1967)23.
13. B.M.Lepinskikh, I.T.Sryvalin, A.A.Tekhomorov, Russ.J.Phys.Chem., 40(1966)840.
14. A.T.Dinsdale, Calphad, 15(1991)317.
15. J.Lacaze, B.Sundman, Metall.Trans., 22A(1991)2211.
16. D.Kevorkov, R.Schmid-Fetzer, F.Zhang, J.Phase Equilib.Diffus.,

25(2004)140.
17. I.Ansara, A.T.Dinsdale, M.H.Rand, Cost 507: Thermochemical database for light metal alloys, Vol. 2, Luxembourg: Office for Official Publications of the European Communities, Belgium, 1998, p.195.
18. O.Redlich, A.T.Kister, Ind.Eng.Chem., 40(1948)345.
19. I.Ansara, B.Sundman, P.Willemin, Acta Metall., 36(1988)977.
20. I.Ansara, N.Dupin, H.L.Lukas, B.Sundman, J.Alloys Compd., 247(1997)20.
21. B.Sundman, B.Jansson, J.O.Andersson, Calphad, 9(1985)153.
22. Y.Du, R.Schmid-Fetzer, H.Ohtani, Z.Metallkd., 88(1997)545.
23. J.Grobner, R.Schmid-Fetzer, A.Pisch, G.Cacciamani, P.Riani, N.Parodi, G.Borzone, A.Saccone, R.Ferro, Z.Metallkd., 90(1999)872.
24. J.Grobner, D.Mirkovic, R.Schmid-Fetzer, Acta Mater., 53(2005)3271.